Experimental characterization of a solar multi-effect distillation system: empirical correlations

Aicha Chorak[1, 2], Patricia Palenzuela[3*], Diego-César Alarcón-Padilla[3], Abdellatif Ben Abdellah [1,2]

[1]Abdelmalek Essaâdi University, Faculty of Science and Technology of Tangier, Ziaten. BP: 416, Tangier, Morocco;
[2]International University of Rabat, Technopolis Rabat-Shore Rocade, Sale, Morocco;
[3]CIEMAT-Plataforma Solar de Almería, Ctra. de Senés s/n, 04200 Tabernas, Almería, Spain
*Corresponding author. E-mail address: patricia.palenzuela@psa.es

Abstract

In the last three decades, developments in desalination plants have been focused on the minimization of its energetic consumption and cost. Advancements include emerging technologies that make use of low grade thermal energy, like Multi-Effect Distillation (MED). The energy optimization of MED systems and their coupling with solar thermal technologies have been deeply investigated by the Solar Desalination Unit of the Plataforma Solar de Almería (PSA) through a solar desalination test facility consisting in a MED plant coupled to a static solar field. Recently, the previous solar field composed of compound parabolic concentrators (CPC) has been replaced by a new one with large-aperture flat plate collectors (FPC). In this work, an experimental characterization of the solar MED system under off-design conditions is presented and discussed. The efficiency of the FPCs' solar field at several temperature levels for different climate conditions and the influence of the variation of key parameters by which the MED plant is controlled (the inlet hot water flow rate and temperature, the feed water flow rate and the condenser temperature) on the freshwater production and performance ratio were analysed with an experimental campaign of 82 experiments. The results obtained were used to fit polynomial expressions that predict the distillate yield and the PR for different operation strategies. The empirical correlations have been validated statistically by the following parameters: R^2, R^2_{adj}, $RMSE$ and SS_E.

Keywords: Large-aperture flat plate collectors; Multi-effect distillation; Off-design experimental analysis; Solar desalination; Empirical correlations

1. Introduction

Due to the geographic coincidence of regions that present water stress and usually have high levels of solar irradiation, seawater desalination processes driven by solar energy seem to be the most promising option to solve the fresh water problems in these zones. For large-scale desalination systems, the best option is indirect desalination systems, which consist on the coupling of a conventional desalination system with the most suitable solar conversion system according to the energy required by the desalination process. Among the distillation methods more frequently used in indirect solar desalination plants, multi-effect distillation (MED) is being preferred due to its low top brine temperature (TBT) and its high thermodynamic efficiency. In 2006, a unique experimental facility for the evaluation of solar MED systems was erected within the framework of the AQUASOL Project with the aim of developing an improved-cost and energy-efficient solar MED system [1]. A solar field composed of compound parabolic concentrators (CPC) with water-based thermal energy storage was the external energy source required by the MED unit. The solar field and the thermal storage system have been recently replaced by a new solar system, consisting of a large-aperture flat

plate collector's solar field with theoretically higher efficiency at the operation temperature of the MED plant, and a doubled-size water tank storage.

The experimental characterization of solar MED processes under design and off-design conditions can be a benchmark for energetic and cost optimization processes together with the research of the most suitable control strategies of other solar MED plants. The literature related to the experimental characterization of solar MED plants is scarce, and most of the studies focused on modeling and single optimization of MED systems have not been supported by experimental data. Blanco et al. [1] carried out an experimental campaign to evaluate the efficiency of a pilot PSA MED plant coupled to a solar field composed with 500 m^2 of CPCs. Results showed that the overall measured efficiency of the solar collectors' field was around 50%. Moreover, they found that the optimum operation temperature of the MED first effect should be between 64-67 ºC which means a specific energy consumption of roughly 60 $kW_{th}h/m^3$. El-Nashar [2] developed a simplified simulation program for predicting the part-load performance of small capacity MED units using hot water as thermal energy source. The model was validated by an exhaustive test campaign carried out in a pilot MED plant located in Abu Dhabi. The simulations were performed at different operating conditions to study the influence of various parameters on the production and the energy consumption of the plant. Results showed that increasing the feed water flow and keeping the value of heating water flow rate constant results in a small increase of distillate production compared with the rise achieved by increasing the heating water flow rate. Fernández-Izquierdo et al. [3] conducted an off-design experimental analysis in the PSA MED plant with few tests varying the hot water temperature entering the first effect. The results showed that the design of a solar system for driving the SOL-14 unit should be based on the recommended conditions of 68 °C of temperature of the thermal input in case of maximizing the performance ratio, PR (which is defined as the mass (in kg) of distillate produced by the thermal energy supplied to the process normalized to 2326 kJ (1000 Btu) that is the latent heat of vaporization of water at 73 °C [4]) and 72 °C in case of maximizing the distillate production. Dongfeng Zhao et al. [5] analyzed theoretically a MED system that works with high-salinity wastewater from a thermal and economic point of view. Results showed that the Gain Output Ratio, GOR (which is defined as the mass ratio between the distillate produced and the steam provided to the system [2]) rises significantly when the vapor temperature in the MED plant last effect is increased. Finally, Xue et al. [6] developed a mathematical model of a backward feed MED plant dealing with high-salinity wastewater in order to evaluate the effect of certain operating parameters on the GOR and on the total heat transfer areas of the MED unit. Results showed that on one hand, the GOR rises slightly with the last effect vapor temperature but in this case the total heat transfer areas increase considerably. On the other hand, they found that the GOR decreases with the rise of feed salinity Georgiou et al. [7] evaluated experimentally the performance of a MED unit in low seawater flow conditions through the evaluation of several parameters, like are the input thermal power and the inlet seawater flow rate and temperature. The main results showed that there is a maximum performance ratio for every thermal power and also that the efficiency of the plant increases with the increase in the seawater feed temperature. Furthermore, the authors proved that the PR increased by 0.7 if one more effect was added to the plant. Some research has also been performed on parametric studies in MED plants dealing with wastewater of petrochemical companies. For example, Zhao et al. [8] determined the optimal operation parameters of a pilot MED plant that is fed with waste water from a petrochemical enterprise. Experimental results demonstrated that the Concentration Ratio (CR), which is defined as the ratio between the discharging salinity and the feedwater salinity, and the GOR would rise up by increasing the number of effects, the steam mass flow rate, and the feedwater temperature while they decreased by increasing the salinity and feedwater flow rate.

This paper presents a complete experimental characterization of a solar desalination system located at the PSA, consisting of a MED unit coupled to a solar field composed of large-aperture flat plate collectors through a water storage system. The experimental campaign has been addressed along the different seasons and the assessment of the energetic efficiency of the solar field as well as the MED unit has been carried out in order to find the optimum operating conditions under different scenarios.

The present paper is arranged as follows: section 2 is dedicated to material and methods and includes a detailed description of all components of the system and an explanation of the methodology employed to characterize both systems, the solar field and the MED plant. Section 3 deals with the experimental results and discussion, which is divided into three parts: firstly, the assessment of the efficiency of flat plate collectors' solar field is presented at several temperature levels for different climate conditions. Secondly, the steady-state results of the MED plant working at off-design conditions are discussed in three scenarios that show: the effect of feed water mass flow rate (m_f), the hot water mass flow rate (m_{hot}), and the vapor temperature in the condenser (T_c) on the distillate production and on the PR of the plant. Thirdly, parametric equations were successfully developed and validated statistically in each case in order to predict the distillation production and the PR using a large range of validation. The last section gives some conclusions withdrawn from this experimental work.

2. Material and Methods

Figure 1 depicts the general layout of how the components of the experimental facility are integrated. The coupling of the MED plant with the solar field is as follows: the water is heated through the solar field and then transfers its thermal energy to the thermal storage circuit through a plate heat exchanger. Then, the hot water from the hot storage tank enters the first effect of the MED desalination plant, being the temperature controlled by a three-way valve (V1). All the components of the solar desalination facility are explained in detail below.

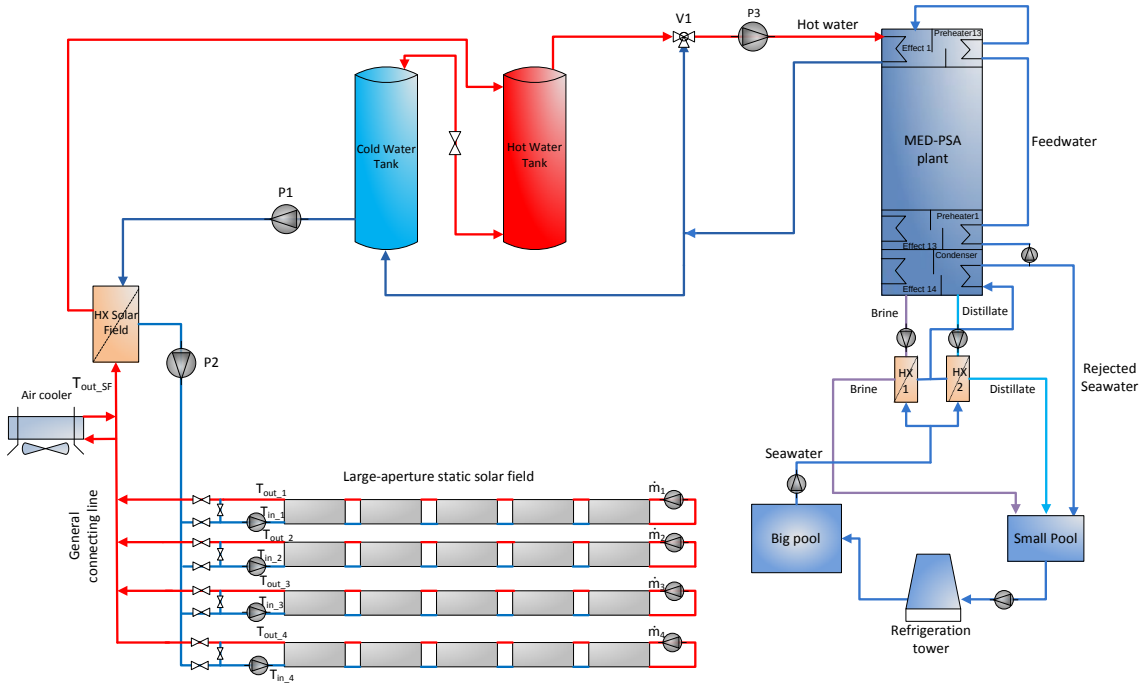

Figure 1. Layout of the solar desalination facility at the PSA

2.1 Solar field

The static solar field (see some pictures in Figure 2), manufactured by Wagner & Co. is composed of 56 flat plate collectors (FPC) type LBM10 with a total aperture area of 565.6 m^2. It consists of 4 loops with 14 large-aperture flat plate collectors each (two rows connected in series per loop with 7 collectors in parallel per row), all of them tilted 35º south orientation. Each loop has its own filling/emptying system consisting in two deposits, from which the heat transfer fluid (water with anti-freeze) is pumped to the collectors starting the operation and where all the water volume in the collectors is spilt either ending the operation or when reaching out a temperature limit (above 100 ºC).

The solar field has flow control valves that permit to have an equal distributed flow rate. Also, the facility has an air cooler (type EAS6-30634/VI, 3*1.55 kW) that allows the entire energy dissipation from the solar field, which is useful for efficiency tests at different temperature levels. The four loops of collectors constitute the primary circuit of the solar desalination facility (see Figure 1) and they are connected with a thermal storage system (secondary circuit) through a heat exchanger (type CB76-100H). The installation is equipped with temperature and pressure sensors and flow meters that collect the experimental data every second.

The LBM10 Flat Plate collector was tested according to European standards UNE-EN 12975 and certified by SolarKeymark, giving the main results shown in Table 1.

Table 1
Dimension, characteristics, and performance of the flat plate solar collectors

Parameter	Symbol	Value
Dimension		
Area (m^2)	A	565.6
Characteristics		
Admitted maximum operating pressure (bar)	P	10
Tilt angle (°)	β	10-85
Weight (kg)	M	218
Heat transfer liquid	L	Water with antifreeze (mixing ratio as needed)
Performance		
Optical efficiency (%)	η_o	83
Heat loss coefficient (W/m^2K)	k_1	3.523
Temperature dependence of the heat loss coefficient (W/m^2K^2)	k_2	0.015

a) b)

c)

Figure 2. Flat plate collectors' solar field at the PSA

2.2 Thermal energy storage

The thermal energy storage (TES) system consists of two water tanks connected to each other with a total storage capacity of 40 m^3 and located between the solar field and MED plant (see Figure 1 and Figure 3). This volume allows an operational autonomy of about two hours to operate the MED plant during intermittent cloudy periods. Also, the TES acts as heat buffers for the regulation of the water temperature at the inlet of the desalination plant. The tanks are made of carbon steel with epoxy inner coating in order to reduce the heat losses and the working fluid, in this case, is water but without anti-freeze. The secondary circuit also counts with four expansion vessels to absorb the increase of the volume of water when it is heated.

Figure 3. Thermal storage tanks installed at PSA

2.3 Multi-effect distillation pilot plant

The thermal desalination unit at the PSA is a forward-feed MED plant with 14 stages or effects, arranged vertically with the maximum pressure and temperature in the top (see Figure 4 (a)). The MED process consists on a series of seawater evaporation-vapor condensation processes that occur in the tube bundles of the effects (called evaporators). The thermal energy source for each effect is the vapor generated in the previous one, except to the first one that is driven by an external energy source. This external energy source is in the form of sensible heat by hot water from the storage system (see Figure 1). The distillate generated in each effect corresponds to the condensation of the vapor that comes from the previous effect. In the case of the last effect, the vapor produced in the evaporator is condensed in a once-through heat exchanger called end condenser. This condenser is refrigerated by a greater volume of seawater than that needed in the process. Apart from the distillate, another sub-product from the process is the brine, which corresponds to the un-evaporated seawater from each effect that is more and more concentrated in salts.

The vacuum system of the MED at the PSA consists of two hydro ejectors, one for effects 2 and 7 and another one for the end condenser. Besides, this system removes the non-condensable gases and the airleakages (as a result of non-perfect air tightness) [9]. The MED unit operates in a closed circuit consisting of two pools (see Figure 4 (c) and (d)). The refrigerated water from the outlet of the condenser, the total distillate water and the total brine from the plant are sent and mixed in the small pool that is connected with a big one, from which the seawater is pumped to the plant as feed source (as refrigerated water and as a feedwater for the distillation process). In order to keep the feed source to the MED plant at a constant temperature, there is a refrigeration tower at the outlet of the small pool (see Figure 1 and Figure 4 (b)). Table 2 shows the operational parameters and specifications of the MED unit at nominal conditions.

Table 2
Operational parameters and specifications of the MED unit at nominal conditions

Parameters	Value
Capacity	72000 L/day
Number of effects	14
Number of preheaters	13
Material of the tube bundles of evaporators, pre-heater and condenser	90-10 Cu-Ni
Hot water flow rate	12 L/s
Sea-water flow	8 m^3/h
Brine reject	5 m^3/h
Distillate production	3 m^3/h
Seawater flow at condenser:	
at 10 °C	8 m^3/h
at 25 °C	20 m^3/h
Heat source energy consumption	190 kW
Vacuum system	Hydro-ejectors (seawater at 3 bar)
Top brine temperature	70 °C
Condenser temperature	35 °C

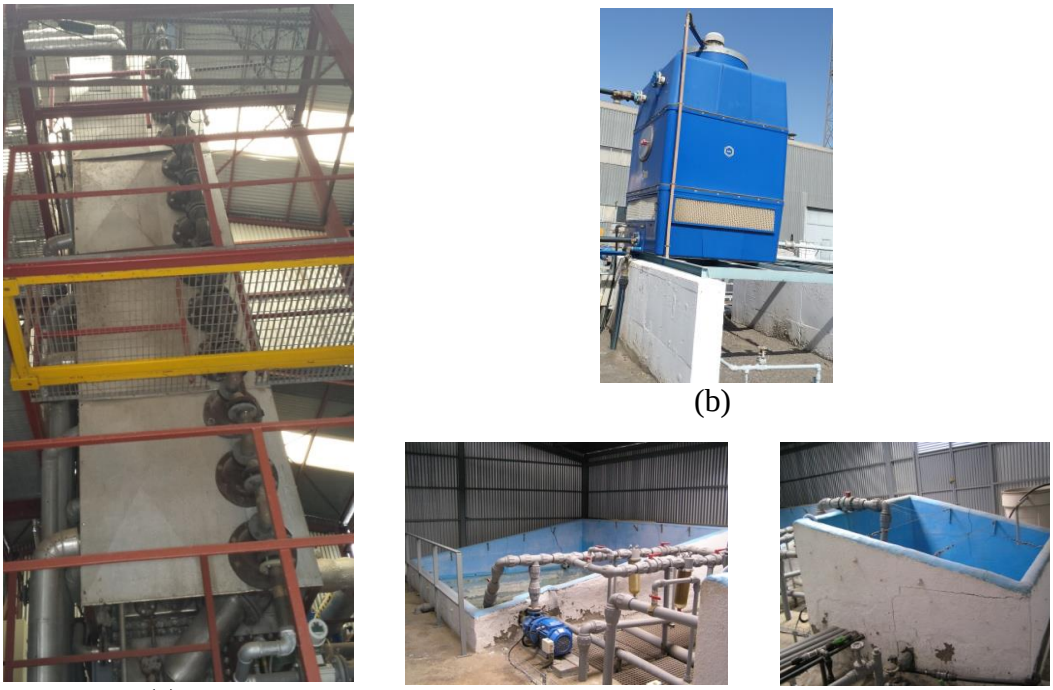

Figure 4. Front view of the MED unit (a), the refrigeration tower (b), the big pool (c) and the small pool (d) at PSA

2.4 Solar collector field and MED plant characterization

2.4.1 Solar Collector Field characterization

The evaluation of the solar field efficiency has been carried out at different outlet water temperatures ($T_{out,SF}$), from 65 °C to 95 °C. For this purpose, the primary circuit is operated as follows: the 4 by-pass valves systems in each loop are opened (while the connecting valves to the general line are closed) and the loops are filled completely with water. After around 10 minutes, each pumping system is activated and the flow rate is adjusted to their design values (37 L/min for four loops). Once the stable conditions are achieved, the valves of the general connecting lines are opened (while the by-pass valves are closed) and P2 is also activated at 100% capacity. In order to achieve a constant $T_{out,SF}$ at a certain value, the speed of the fans of the air cooler is adjusted accordingly, and the measurements are taken once the steady state conditions are reached. During the experiments, the inlet and outlet temperatures and the flow rates of each loop and of the general connecting line were monitored as well as the ambient temperature (T_{amb}) and the global solar irradiance (G_T). The temperatures were measured with Pt100 TR10 class C in all cases in the FPC solar field. The flow rates were measured by electromagnetic flow meters Promag 50P15 in the case of loop 1, Promag 10P25 in loops 2, 3, 4 and 5, and Promag 10P32 in the general connecting line. Finally, a precision pyranometer (CM 6B) records the meteorological data including the global solar radiation and the ambient temperature which was measured by a Pt 1000IEC 751 1/3 Class B that is shown in Figure 5.

Figure 5. Pyranometer at the PSA

On one hand, the theoretical efficiency is determined according to the European Standard UNE-EN 12975-2 by the following equation [10]:

$$\eta_{th} = (\eta_0 \cdot K_{\tau\alpha}) - k_1 \cdot \frac{T_{col} - T_{amb}}{G_T \cdot C} - k_2 \cdot G_T \cdot \left(\frac{T_{col} - T_{amb}}{G_T \cdot C}\right)^2 \quad (1)$$

The parameters of the curve were already described above (see Table 1).
$K_{\tau\alpha}$ is the incidence angle modifier defined as the ratio of τα (which is the transmittance-absorptance product) measured at some incident angle θ of the incoming light to the value of (τα) at normal incidence $(\tau\alpha)_n$, and it is determined by the following general empirical expression that is widely used for FPCs [11]:

$$K_{\tau\alpha} = 1 - b_o \cdot \left(\frac{1}{cos\theta} - 1\right) \quad (2)$$

where b_o is a constant called incidence angle modifier coefficient and θ is the incidence angle defined as the angle between the beam solar radiation and the normal to the collector surface.
T_{col} is the average fluid temperature in the collector between the inlet (T_{in}) and the outlet (T_{out}) (in the case of the solar field at PSA it would be the average fluid temperature in the loop), as given:

$$T_{col} = \frac{T_{in} + T_{out}}{2} \quad (3)$$

Finally, C is the concentration factor that is 1 in the case of flat plate collectors.

On the other hand, the experimental efficiency was determined based on the thermal performance of the collectors, which is defined as the ratio of the useful energy gain by the solar FPCs and the irradiance reaching their aperture area, and it is given by the following equation [12]:

$$\eta_{ex} = \frac{\dot{Q}_U}{G_T.A} = \frac{\dot{m} \cdot \left(h_{out\_FPCs} - h_{in\_FPCs}\right)}{G_T \cdot A} \quad (4)$$

Where $\dot{m}$ is the flow rate of each loop, h_{in_FCPs} and h_{out_FPCs} are the enthalpy at the inlet and outlet of each loop, respectively, and A is the total the aperture area of the solar field.

2.4.2 Multi-effect Distillation Plant characterization

The characterization of the MED plant was carried out by the study of the influence of the variation of all the parameters by which the operation of the MED system is controlled, on the distillate production and the PR. The latter parameter determines the thermal efficiency of a MED plant and it is expressed by the following equation:

$$PR = \frac{\dot{m}_d . 2326}{Q_h} \tag{5}$$

where $\dot{m}_d$ is the distillate production and Q_h is the thermal energy consumption of the MED plant. The latter is calculated using the enthalpy difference at the inlet (h_{inMED}) and outlet (h_{outMED}) of the first tube bundle of the MED unit at the hot water inlet and outlet temperatures (T_{in} and T_{out}, respectively), and the hot water flow rate (m_{hot}) through this tube bundle, as follows:

$$Q_h = m_{hot} . \left(h_{in_{MED}} - h_{out_{MED}}\right) \tag{6}$$

Three experimental campaigns (82 tests in total) were carried out for the exhaustive characterization of the solar MED pilot plant, which are detailed below:

- Case study 1: m_f was varied between 5 m^3/h and 9 m^3/h for every hot water inlet temperature (T_{hot}) in the first effect, from 62 °C to 74 °C. In these tests, m_{hot} and T_c were fixed at 12 L/s and at 35 °C, respectively.
- Case study 2: $m_{hot}$was varied between 7 L/s and 14 L/s for every T_{hot} in the first effect, from 60 °C to 74 °C. In this case, T_c was fixed at 35 ºC and m_f at 8 m^3/h.
- Case study 3: T_c was varied between 25 °C and 35 °C for every T_{hot}, from 60 °C to 74 °C. In this experiments, m_{hot} and m_f were kept fixed at 12 L/s and 8 m^3/h, respectively.

All the measurements were taken after steady state conditions were reached in the solar desalination system and the average value of each variable was determined. An error analysis was performed taking into account the measurements uncertainty of all the instruments and equipment and the standard deviation. Due to the fact that the PR is an indirect parameter determined by direct measures, an uncertainty propagation analysis has been carried out so as to quantify the goodness of the PR results. For this purpose, a tool of the Engineering Equation Solver software described in [13] has been used.

Table 3 shows the measurement uncertainties of the distillate water mass flow rate ($\dot{m}_d$), m_{hot} and T_{hot} (all of them direct variables).

Table 3
Measurements uncertainty of the direct variables

Parameter	Symbol	Measurement uncertainty
Hot water temperature	$U_{T_{hot}}$[°C]	0.85
Hot water flow rate	$U_{\dot{m}_{hot}}$[L/s]	0.5%

Distillate water mass flow rate	$U_{\dot{m}_d}$[kg/s]	0.75%

Thermophysical properties of water vapor were calculated with XSteam Excel v2.6 according to IAPWS IF 97 [14, 15].

3. Experimental results and discussion

3.1. Solar field efficiency

Figure 6 shows different experiments carried out to evaluate the experimental and theoretical efficiency of the FPC solar field along the daylight hours, keeping the solar field outlet temperature ($T_{out,SF}$) at 65 ºC, 70 ºC, 75 ºC, 80 ºC, 85 ºC, 90 ºC and 95 ºC. As it is observed, the difference between the experimental and theoretical efficiencies is higher early in the morning and after solar noon because of the influence of the incidence angle modifier, which varies along the day due to the static nature of the solar collectors. In all cases, the experimental efficiency is lower than the theoretical one. It could be due to either the thermal losses in piping and tanks or to the lower performance of solar collector field. The maximum instantaneous experimental and theoretical efficiency of the FPC solar field was found at $T_{out,SF}$ of 65 ºC and it had a value about 62.7% and 62.9% at 11:49:32 and 12:35:31, respectively.

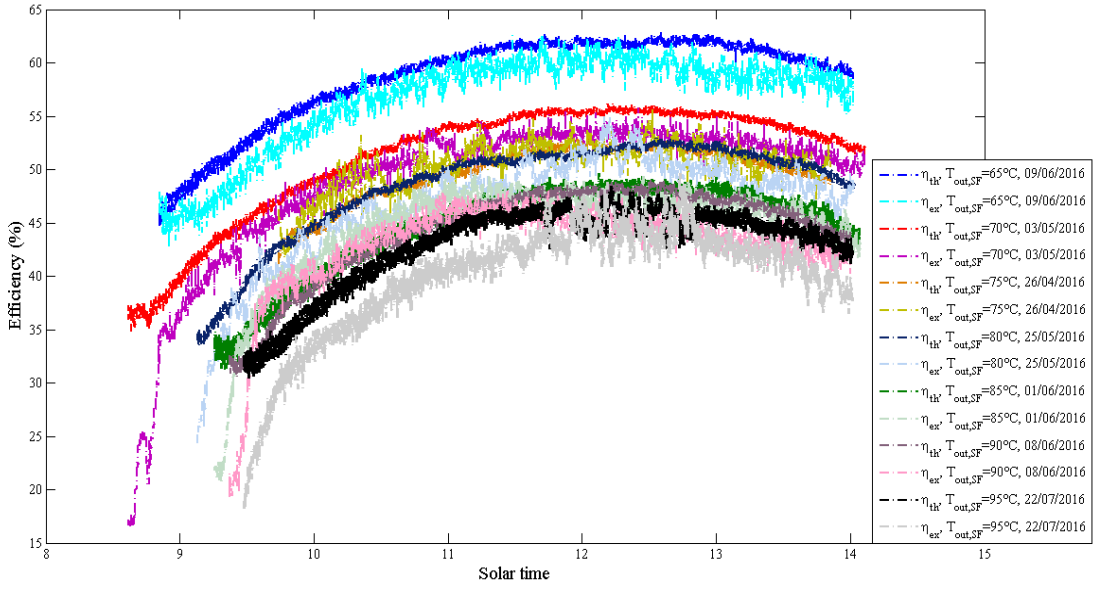

Figure 6. Theoretical and experimental solar field efficiency at different hot water outlet temperatures and at several days (09/06/2016, 03/05/2016, 26/04/2016, 25/05/2016, 01/06/2016, 08/06/2016 and 22/07/2016)

The average values of experimental and theoretical efficiency ($\eta_{ex-mean}, \eta_{th-mean}$) of the solar field efficiency tests, the maximum experimental efficiency (η_{ex-max}), the average T_{amb}, and the average G_T are shown in Table 4 for each case. The respective minimum and maximum experimental mean efficiency of the solar field was 39.8% in July at $T_{out,SF}$ of 95 ºC and 57.0% in June at 65 ºC. Similarly, the minimum and maximum theoretical mean efficiency were 42.9 % and 58.9%, respectively.

Table 4
Comparison of the results of the solar field efficiency for different temperature levels

$T_{out,SF}$ [°C]	T_{amb} [°C]	*Test*	$\eta_{ex-mean}$ [%]	$\eta_{th-mean}$ [%]	η_{ex-max} [%]	G_T [W/m^2]
95	35.9	22/07/2016	39.8	42.9	49.7	807.6
90	35.1	08/06/2016	42.9	44.4	48.0	795.0
85	28.2	01/06/2016	44.5	44.7	49.6	853.4
80	30.3	25/05/2016	46.8	48.5	55.0	828.0
75	19.3	26/04/2016	46.7	47.0	55.6	800.7
70	19.7	03/05/2016	50.2	52.2	55.8	795.0
65	36.6	09/06/2016	57.0	58.9	62.7	777.5

Figure 7 shows the operation of the solar field for several tests at different $T_{out,SF}$ (95 ºC, 85 ºC, 75 ºC and 65 ºC) in order to have an idea of the thermal power that can be delivered by the solar field to the desalination process. Also, Table 5 shows a summary of the results obtained in terms of energy supplied by the solar field along the day ($E_{supplied}$), the hours of thermal storage ($t_{storage}$) that allow to cover the operation of the MED plant (including the transient periods in which there are clouds or in the start-up), the peak thermal power (P_{max}), the remaining thermal power ($P_{remaining}$) that is used to load the tanks and the ambient temperature (T_{amb}) for different temperature levels. Results revealed that the solar field is able to produce much more thermal power than needed by the MED plant through the day, with a maximum value at 65 ºC of 304.0 kW_{th}, so the remaining 114.0 kW_{th} are stored in the water tanks. In this case, the total thermal energy provided by the solar field was of 1157.4 kWh, which allows 6 hours of storage to cover the operation of the MED plant at this temperature level.

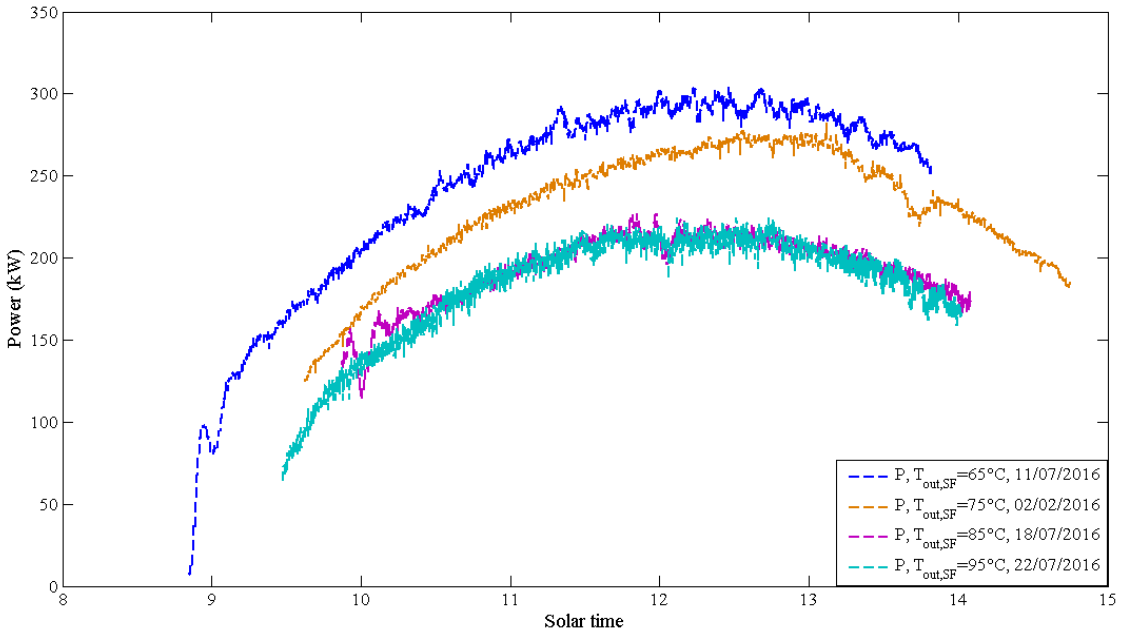

Figure 7. Power provided by the solar collector field for several days and at different solar field outlet temperature *vs* the solar time

Table 5
Comparison results of the energy supplied during the day by the FPCs, the storage time, the peak thermal power, the remaining thermal power and the ambient temperature for different temperature levels

T_{out_SF} [°C]	T_{amb} [°C]	*Test*	$E_{supplied}$ [kWh]	$t_{storage}$ [h]	P_{max} [kW_{th}]	$P_{remaining}$ [kW_{th}]
95	35.9	22/07/2016	827.7	4.4	224.7(at 12:00:46 with 818.8W/m^2)	34.7
85	30.1	18/07/2016	849.1	4.5	228.8 (at 11:51:02 with 880.6 W/m^2)	38.8
75	19.8	02/02/2016	1081.8	5.7	282.0 (at 13:06:58 with 870.2 W/m^2)	92.0
65	35.2	11/07/2016	1157.4	6.1	304.0 (at 12:22:24 with 835.9 W/m^2)	114.0

3.2. Steady-state characterization of the MED plant

Case study 1: Influence of the variation of the feed water flow rate on the water production and the PR

Figures 8 and 9 show the distillate production and PR obtained for different m_f and different T_{hot}. Tables 6 and 7 show the numerical values of the distillate production and the PR obtained in the experimental campaign with the corresponding errors. Also, the percentages increase/decrease that these variables present with the variation in m_f for each T_{hot} are shown.

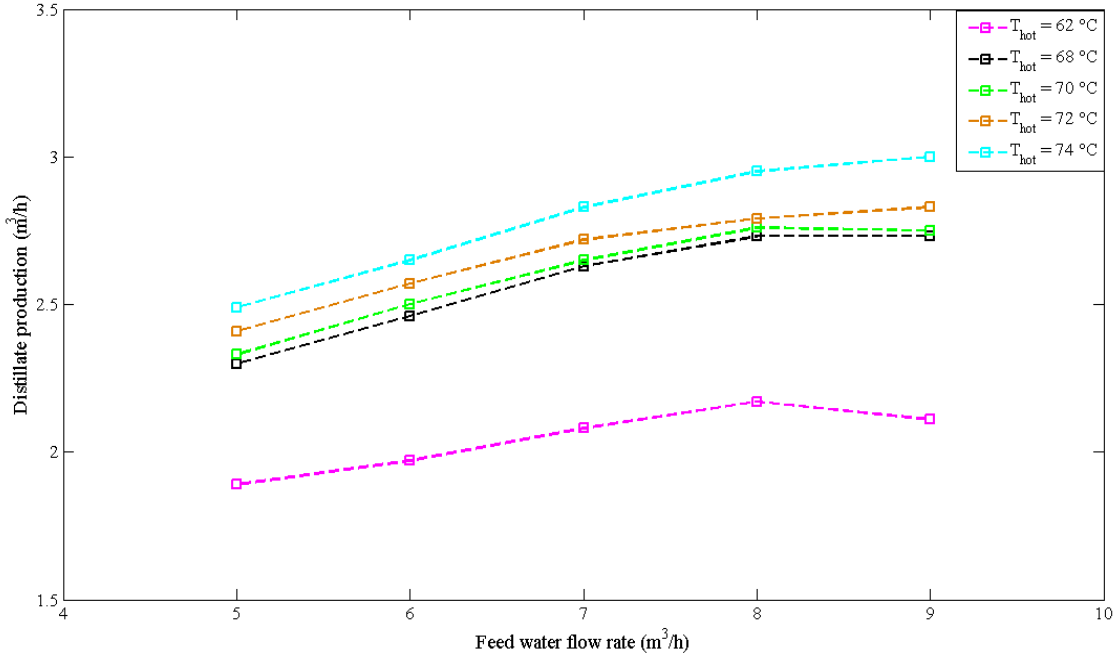

Figure 8. Variation of the distillate production from the MED-PSA plant with different feed water flow rates (5-9 m^3/h) for several hot water inlet temperatures (62-74 ºC)

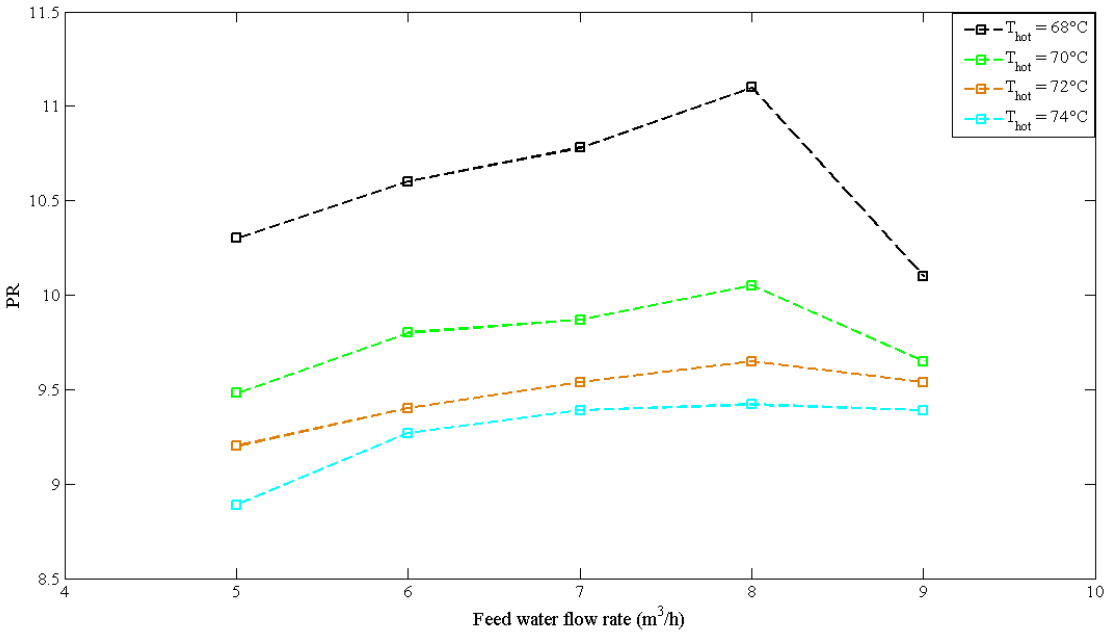

Figure 9. Variation of the Performance Ratio of the MED-PSA plant with different feed water flow rates (5-9 m^3/h) for several hot water inlet temperatures (68-74 ºC)

In Figure 8, it can be observed that, as expected, the distillate production rises with T_{hot} in all cases. It also increases with the rise of m_f from 5 m^3/h to 9 m^3/h but this rise is different depending on the temperature of the heat source supply in the first effect. As observed in Table 6, the distillate production increased with a higher percentage at T_{hot} above 68 ºC and this increase drops significantly for low hot water temperatures. The maximum rise in the distillate production (20.72%) was reached at T_{hot} of 74 ºC, when m_f was increased from 5 to 9 m^3/h. It was also observed that the rate of growth in the distillate production decreases for all T_{hot}values at m_f above 8 m^3/h. Even in some cases (T_{hot} of 62 ºC and 70 ºC) the distillate

production decreases the higher m_f is, especially at 62 ºC that decreased with a percentage of 2.74%. This decrease could be caused by the shorter contact time in this case between the feed and the heating surface of the horizontal tube, which decreases the amount of heat absorbed by the saturated feed water in the falling film evaporation process. The maximum amount of distillate is reached (3 m^3/h) when m_f is 9 m^3/h and T_{hot} the one at nominal conditions of the MED plant (74 ºC). According to the results, it can be stated that even at higher m_f, the production of the MED plant does increase significantly.

Regarding the PR, it should be highlighted that the accuracy of the performance ratio is strongly dependent on the accuracy of T_{hot} and flow measurements, so a small error in these measurements yields a much higher error in the PR calculation. This is why some experimental points have been discarded in the three case studies. In Figure 9, it can be observed that the PR decreases with the rise of T_{hot} which is in agreement with the work published in [16], and increases with the rise of the m_f which is in agreement with other works of the literature [17], in this case until 8 m^3/h. For example, in the case when m_f was 5 m^3/h, the PR at 74 ºC was 1.16% lower than at 68 ºC. As observed in Table 7, the increase in the PR with the growth of m_f from 5 to 8 m^3/h was very similar for all hot water temperatures. The trend changes at higher m_f, resulting in a decrease of the PR. This decrease is especially significant at 68 ºC.

The significant increase in both parameters, the distillate production and the PR, with m_f from 5 m^3/h to 8 m^3/h can be because the increment of m_f helps to strengthen the convective heat transfer of the external falling film evaporation, increasing then the overall heat transfer coefficient and in consequence the distillate produced and the PR.

Table 6
Average values of the experimental results of distillate production with the measurements errors, and the percentage increase/decrease with the feedwater flow rate

Hot water inlet temperature (°C)	Feed water flow rate (m^3/h)	Distillate production (m^3/h)	Percentage increase in $\dot{m}_d$ with m_f (5-9 m^3/h)	Percentage decrease in $\dot{m}_d$ with m_f (8-9 m^3/h)
74	5	2.49±0.07		
74	6	2.65±0.10		
74	7	2.83±0.08	20.72%	
74	8	2.95±0.07		-1.63%
74	9	3.00±0.08		
72	5	2.41±0.07		
72	6	2.57±0.07		
72	7	2.72±0.08	17.61%	
72	8	2.79±0.08		-1.38%
72	9	2.83±0.08		
70	5	2.33±0.08		
70	6	2.50±0.06		
70	7	2.65±0.08	18.36%	
70	8	2.76±0.08		0.25%
70	9	2.75±0.07		
68	5	2.30±0.11		
68	6	2.46±0.11	18.95%	
68	7	2.63±0.08		

68	8	2.73±0.09		-0.11%
68	9	2.73±0.08		
62	5	1.89±0.09		
62	6	1.97±0.08		
62	7	2.08±0.08	11.80%	
62	8	2.17±0.09		2.74%
62	9	2.11±0.08		

Table 7
Average values of the experimental results of PR with the measurements errors, and the percentage increase/decrease with the feedwater flow rate

Hot water inlet temperature (°C)	Feed water flow rate (m^3/h)	PR	Percentage increase in PR with m_f (5-8 m^3/h)	Percentage decrease in PR with m_f (8-9 m^3/h)
74	5	8.89±1.08		
74	6	9.27±1.41	5.98%	
74	7	9.39±1.03		
74	8	9.42±0.91		0.37%
74	9	9.39±1.03		
72	5	9.20±1.06		
72	6	9.40±1.01	4.86%	
72	7	9.54±1.18		
72	8	9.65±1.16		1.15%
72	9	9.54±1.12		
70	5	9.48±1.31		
70	6	9.80±1.02	6.02%	
70	7	9.87±1.18		
70	8	10.05±1.23		4.11%
70	9	9.65±1.00		
68	5	10.30±2.00		
68	6	10.60±1.89	7.77%	
68	7	10.78±1.25		
68	8	11.10±1.50		9.92%
68	9	10.10±1.23		

Case Study 2: Influence of the variation of hot water flow rate on water production and PR

Figure 10 and 11 present the influence of the variation of m_{hot} on the distillate production and the PR, respectively. Also, the numerical results with the measurement errors are shown in Table 8 and 9 together with the percentages increase/decrease that the distillate production and the PR present with the variation in m_{hot} for each T_{hot}.

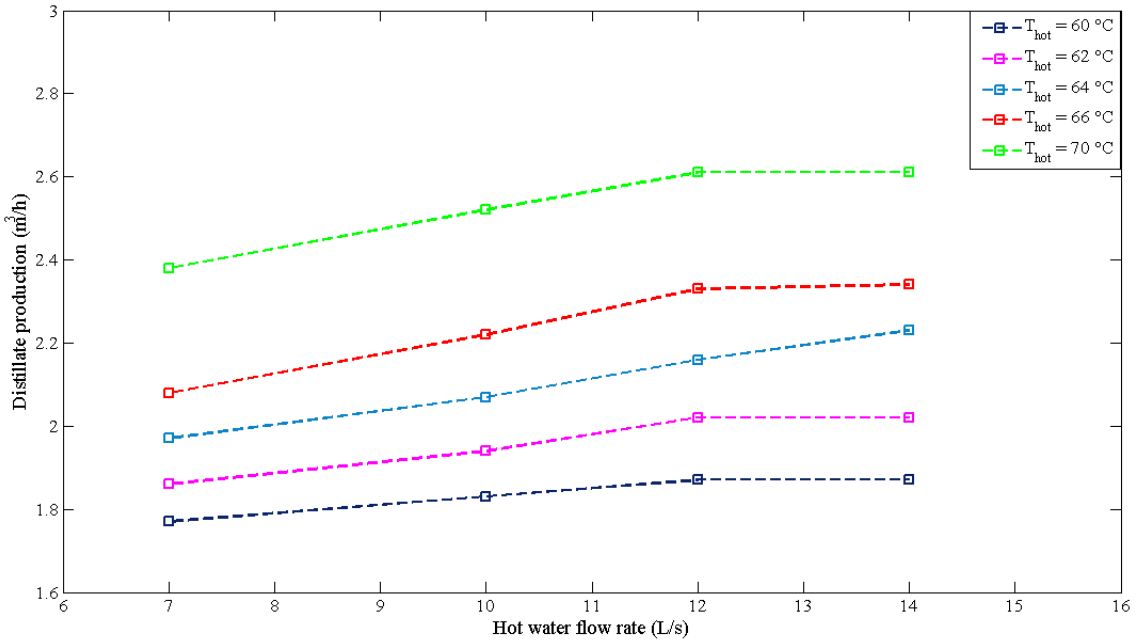

Figure 10. Variation of distillate production from the MED-PSA plant with different hot water flow rates (7-14 L/s) for several hot water inlet temperatures (60-70 ºC)

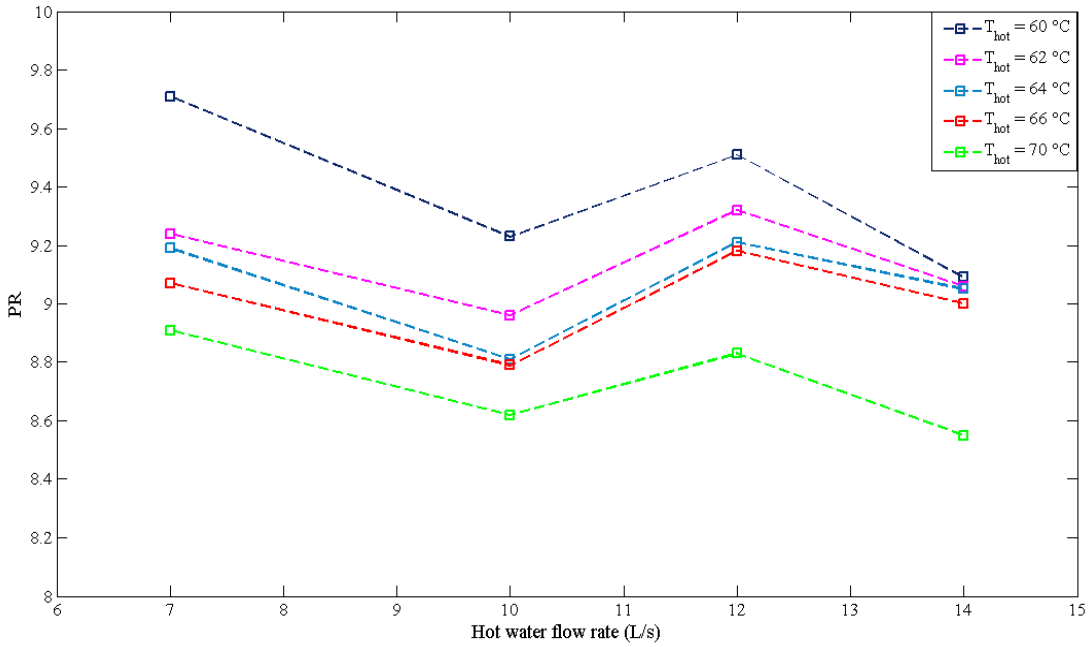

Figure 11. Variation of the Performance Ratio of the MED-PSA plant with the hot water flow rate (7-14 L/s) for several hot water inlet temperatures (60-70 ºC)

As observed in Figure 10, the distillate production increases by increasing either m_{hot} or T_{hot}. This increase is caused by an increase in the rate of vapor formation inside the first effect as a result of a higher thermal power supplied to this effect. It leads to an increase in the vapor produced in the rest of effects and therefore to a rise in the distillate produced by the MED

unit. These results are in agreement with those observed in the works published in [17-19]. As shown in Table 8, with an increase of m_{hot} between 7 L/s and 14 L/s, the distillate production increases a bit more for high T_{hot}. It can also be seen that the growth rate in the freshwater production is much higher from 7 L/s to 12 L/s than from 12 L/s to 14 L/s. The highest increase obtained for a total variation of m_{hot} between 7 L/s and 14 L/s was given at T_{hot} of 64 °C.

According to the data presented in Table 6 and 8, it can be observed that the rise in m_{hot} has less impact on the distillate production compared to the increase in the m_f for the same T_{hot}, which is in good agreement with the work published in [20].

Regarding the effect of the m_{hot} on the PR, Figure 11 shows that the PR decreases slightly for low m_{hot} (from 7 L/s to 10 L/s), and it is higher for larger m_{hot}, which match with other works [17]. As observed in Table 9 the PR increases a percentage around 3-4% when m_{hot} varies from 10 L/s to 12 L/s. This increase can be due to the fact that the evaporative process through the tube bundle is better close to its design value (12 L/s).

For m_{hot} higher than 12 L/s, it was observed a reduction in the PR due to the fact that the rise in the thermal energy consumed is higher than the distillate production. As indicated in Figure 11, the distillate production is maintained practically constant despite the increase in m_{hot} from 12 L/s to 14 L/s (see Table 8 and 9).

Table 8
Average values of the experimental results of distillate production with the measurement errors and the increase percentage of the distillate production with the m_{hot}

Hot water inlet temperature (°C)	Hot water flow rate (L/s)	Distillate production (m^3/h)	Percentage increase in $\dot{m}_d$ with m_{hot}(7-14 L/s)	Percentage increase in $\dot{m}_d$with m_{hot}(7-12 L/s)	Percentage increase in $\dot{m}_d$ with m_{hot} (12-14 L/s)
60	7.00	1.77±0.06	5.68%	5.99%	
60	10.00	1.83±0.06			
60	12.00	1.87±0.06			0.30%
60	14.00	1.87±0.07			
62	7.00	1.86±0.07	8.75%	8.39%	
62	10.00	1.94±0.06			
62	12.00	2.02±0.08			0.34%
62	14.00	2.02±0.07			
64	7.00	1.97±0.07	13.10%	9.61%	
64	10.00	2.07±0.06			
64	12.00	2.16±0.07			3.18%
64	14.00	2.23±0.07			
66	7.00	2.08±0.09	12.65%	12.19%	
66	10.00	2.22±0.07			
66	12.00	2.33±0.07			
66	14.00	2.34±0.08			0.41%
70	7.00	2.38±0.07	10.05%	9.67%	
70	10.00	2.52±0.06			

70	12.00	2.61±0.06			0.35%
70	14.00	2.61±0.06			

Table 9
Average values of the experimental results of PR with the measurement errors and the increase/decrease percentage of the PR with $\boldsymbol{m_{hot}}$

Hot water inlet temperature (°C)	Hot water flow rate (L/s)	PR	Percentage decrease in PR with m_{hot} (7-10 L/s)	Percentage increase in PR with m_{hot} (10-12 L/s)	Percentage decrease with m_{hot} (12-14 L/s)
60	7.00	9.71±1.32			
60	10.00	9.23±1.14	5.26%		
60	12.00	9.51±1.19		3.02%	
60	14.00	9.06±1.26			4.90%
62	7.00	9.24±1.36			
62	10.00	8.96±1.13	3.07%		
62	12.00	9.32±1.54		3.95%	
62	14.00	8.92±1.26			4.46%
64	7.00	9.19±1.31			
64	10.00	8.81±1.06	4.33%		
64	12.00	9.21±1.19		4.47%	
64	14.00	9.05±1.20			1.79%
66	7.00	9.07±1.66			
66	10.00	8.79±1.07	3.16%		
66	12.00	9.18±1.15		4.43%	
66	14.00	9.00±1.17			1.95%
70	7.00	8.91±1.08			
70	10.00	8.62±0.82	3.37%		
70	12.00	8.83±0.80		2.45%	
70	14.00	8.55±0.86			3.24%

Case Study 3: Influence of the variation of the vapor temperature in the condenser on water production and PR

The influence of the variation of T_c on the distillate production and the PR are shown in Figure 12 and Figure 13, respectively. Tables 10 and 11 present the numerical results with the measurement errors and the percentages increase/decrease that the distillate production and the PR present with the variation in T_c for each T_{hot} .

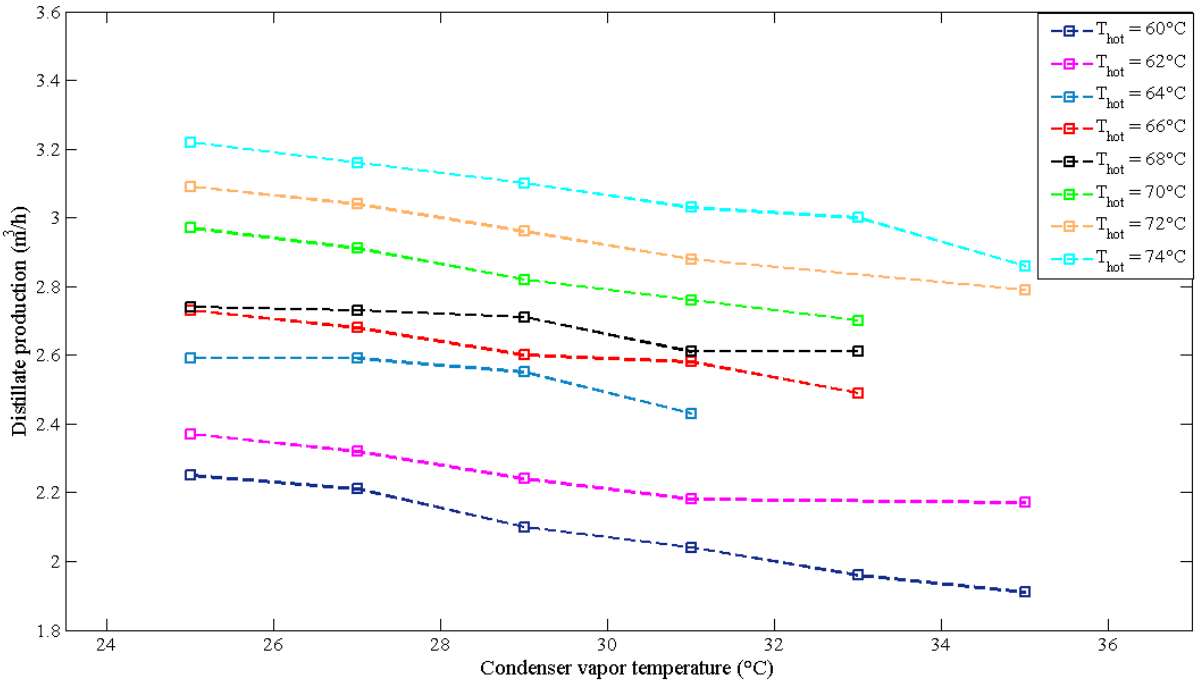

Figure 12. Distillate production of the MED-PSA plant at different condenser vapor temperatures (25-35 ºC) and different hot water inlet temperatures (60-74 ºC)

Regarding the distillate production, Figure 12 shows that it decreases with the increase in T_c from 25 ºC to 35 ºC. The increase in T_c while the vapor temperature of the first effect is fixed (by maintaining T_{hot}constant) makes the temperature difference between effects smaller. This temperature difference is the driving force of the process so its decrease leads to a lower evaporative capacity between effects giving place to a lower distillate production. From Table 10, it can be observed that the decrease in the distillate production is higher for low and high hot water temperatures and smaller for intermediate T_{hot}.

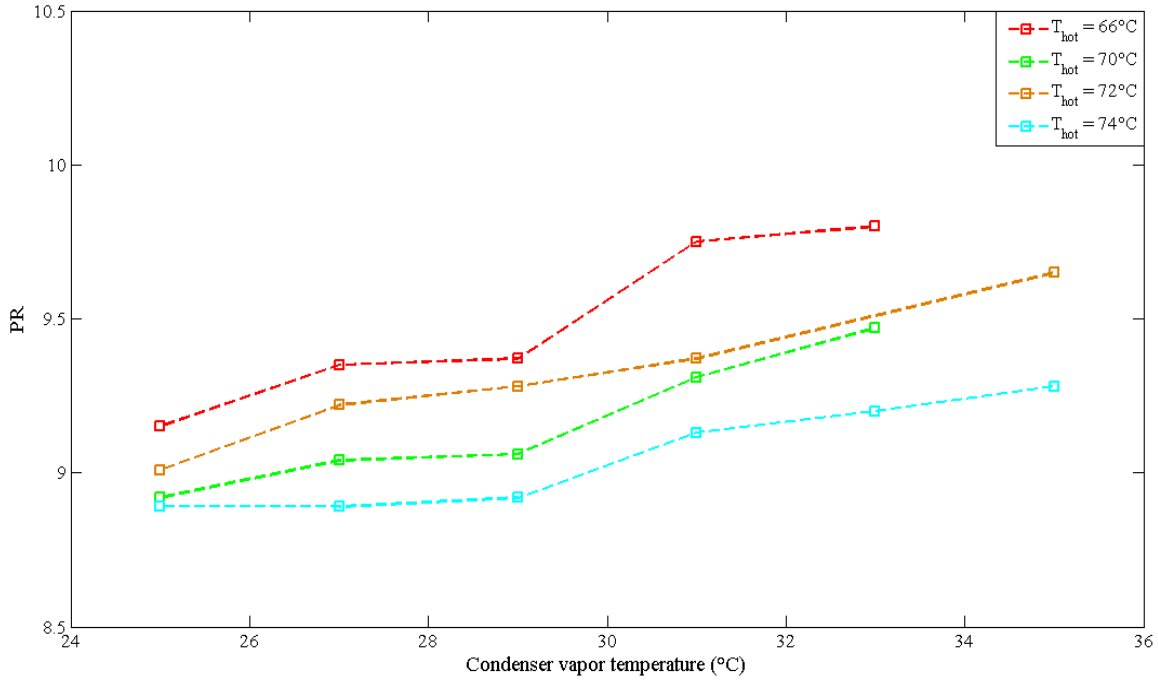

Figure 13. Variation of the Performance Ratio of the MED-PSA plant with the condenser vapor temperature (25-35 ºC) for several hot water inlet temperatures (66-74 ºC)

Regarding the tendency of the PR, Figure 13 shows that it increases with the rise in T_c, which is in agreement with other works of the literature [2, 5]. This rise is due to several factors: the rise in T_c results in a higher feed water temperature at the outlet of the last preheater (located next to the first effect), which leads to a lower thermal consumption and therefore to a higher thermal efficiency of the MED plant; furthermore, as mentioned before, the temperature difference between the adjacent effects becomes smaller and this makes the process more efficient thermodynamically. From Table 11, it was observed that the percentage of increase in the PR with the rise in T_c is reduced at the nominal value of T_{hot} (74 ºC).

Comparing the results of the PR obtained from this case (Table 11) and those ones obtained in the case 1 (Table 7), it can be seen that the rise inm_f has more influence in PR than that of T_c at the maximum hot water temperature. At T_{hot} of 72 ºC, the rise in T_c is more influential over PR, and at 70 ºC and 66 ºC, the effect of T_c and m_f is very similar.

In the case of comparing these results with respect those ones obtained in the case 2 (see Tables 9 and 11), it can be noticed that the rise in T_c has more influence on the PR than the rise in m_{hot} from 10 to 12 L/s at the same T_{hot}.

In the case of the distillate production, comparing the cases 1 and 3 (see Tables 6 and 10), it can be seen that the rise of m_f has more influence on the production of distillate that decreasing T_c considering the same T_{hot}. If cases 2 and 3 are compared (see Tables 8 and 10), it is observed that the increase of m_f has more influence on the distillate production that increasing m_{hot} considering the same T_{hot}.

Table 10
Average values of the experimental results of distillate production with the measurement errors and the increase percentage of the distillate production with the decrease in T_c

Hot water inlet temperature (°C)	Vapor temperature in the condenser (°C)	Distillate production (m^3/h)	Percentage increase of $\dot{m}_d$ with the decrease in T_c (from 33/35 ºC to 25 ºC)
60	25	2.25±0.09	17.97%
60	27	2.21±0.07	
60	29	2.10±0.09	
60	31	2.04±0.07	
60	33	1.96±0.06	
60	35	1.91±0.08	
62	25	2.37±0.10	9.35%
62	27	2.32±0.10	
62	29	2.24±0.09	
62	31	2.18±0.06	
62	33	2.19±0.07	
62	35	2.17±0.09	
64	25	2.59±0.06	

64	27	2.59±0.07	
64	29	2.55±0.07	6.76%
64	31	2.43±0.06	
66	25	2.73±0.10	
66	27	2.68±0.08	
66	29	2.60±0.06	9.57%
66	31	2.58±0.06	
66	33	2.49±0.06	
68	25	2.74±0.11	
68	27	2.73±0.07	
68	29	2.71±0.07	4.64%
68	31	2.61±0.06	
68	33	2.61±0.05	
70	25	2.97±0.10	
70	27	2.91±0.10	
70	29	2.82±0.06	9.84%
70	31	2.76±0.06	
70	33	2.70±0.06	
72	25	3.09±0.09	
72	27	3.04±0.09	
72	29	2.96±0.07	10.71%
72	31	2.88±0.05	
72	35	2.79±0.08	
74	25	3.22±0.05	
74	27	3.16±0.09	
74	29	3.10±0.09	12.41%
74	31	3.03±0.08	
74	33	3.00±0.08	
74	35	2.86±0.07	

Table 11
Average values of the experimental results of the PR with the measurement errors and the increase percentage of PR with the increase of T_c

Hot water inlet temperature (°C)	Vapor temperature in the condenser (°C)	PR	Percentage increase of PR with the increase of T_c (from 25 ºC to 33/35 ºC)
66	25	9.15±1.29	
66	27	9.35±1.11	
66	29	9.37±0.80	7.08%
66	31	9.75±0.89	
66	33	9.80±0.94	

70	25	8.92±1.24	6.15%
70	27	9.04±1.20	
70	29	9.07±0.78	
70	31	9.31±0.84	
70	33	9.47±0.88	
72	25	9.01±1.01	7.10%
72	27	9.22±1.08	
72	29	9.28±0.92	
72	31	9.37±0.68	
72	35	9.65±1.16	
74	25	8.89±0.55	4.43%
74	27	8.89±1.02	
74	29	8.92±1.03	
74	31	9.13±0.93	
74	33	9.20±0.96	
74	35	9.28±0.93	

3.3 Empirical Correlations

Parametric equations were obtained from the experimental data in the three case studies, for the distillation production and the PR. The coefficients of the parametric equations were determined with a confidence level of 95%.

3.3.1 The water production and the PR as a function of the feed water flow rate and the hot water inlet temperature

An empirical correlation of $\dot{m}_d$ and PR as function of both T_{hot} and m_f was developed and these are the parametric equations obtained:

$$\dot{m}_d = -16.2 + (0.473 \cdot T_{in}) + \left(0.09863 \cdot m_f\right) - (0.003303 \cdot T_{in}^2) + \left(0.004976 \cdot T_{in} \cdot m_f\right) - (0.02414 \cdot m_f^2) \quad (7)$$

The expression is adequate for the following parameter ranges:

$60 \leq T_{hot} \leq 74$ ºC
$5 \leq m_f \leq 9\ m^3/s$

$$PR = (221.1) - (5.764 \cdot T_{in}) + (0.1678 \cdot m_f) + (0.03825 \cdot T_{in}^2) + (\ 0.01745\ \cdot T_{in} \cdot m_f) - (0.09554 \cdot m_f^2) \quad (8)$$

Due to the lack of accuracy of the performance ratio at certain temperatures, the range of validity of this variable is lower than that of the distillate:

$68 \leq T_{hot} \leq 74$ ºC
$5 \leq m_f \leq 9\ m^3/s$

3.3.2 Water production and PR as a function of the hot water flow rate and the hot water inlet temperature

An empirical correlation of $\dot{m}_d$ and PR as function of both T_{hot} and m_{hot} was obtained from the experimental data:

$$\dot{m}_d = -0.273 + (0.008409 \cdot T_{in}) - (0.04452 \cdot m_{hot}) + (0.0003093 \cdot T_{in}^2) + (0.001969 \cdot T_{in} \cdot m_{hot}) - (0.002485 \cdot m_{hot}^2) \quad (9)$$

$$PR = 648.2 - (26.74 \cdot T_{in}) - (16.45 \cdot m_{hot}) + (0.3842 \cdot T_{in}^2) + (0.3137 \cdot T_{in} \cdot m_{hot}) + (0.5995 \cdot m_{hot}^2) - (0.001835 \cdot T_{in}^2) - (0.002371 \cdot T_{in}{}^2 \cdot m_{hot}) - (0.0001411 \cdot T_{in} \cdot m_{hot}^2) - (0.01844 \cdot m_{hot}^3) \quad (10)$$

The correlations are valid for the following ranges:

$60 \leq T_{hot} \leq 74\ ^{\circ}C$
$60 \leq m_{hot} \leq 14\ L/s$

3.3.3 Water production and PR as a function of condenser the vapor temperature and the hot water inlet temperature

The polynomial fit of $\dot{m}_d$ and PR as function of T_{hot} and T_c is given by the following equation:

$$\dot{m}_d = -6.717 + (0.232 \cdot T_{in}) - (0.01708 \cdot T_c) - (0.001212 \cdot T_{in}^2) - (4.687 \cdot 10^{-5} \cdot T_{in} \cdot T_c) - (0.00016663 \cdot T_C^2) \quad (11)$$

(12)

$$PR = 0.9205 + (0.1229 \cdot T_{in}) + (0.3414 \cdot T_c) - (0.006089 \cdot T_{in} \cdot T_c) + (0.002579 \cdot T_c^2)$$

The correlations given here are valid over the following parameter ranges:

$60 \leq T_{hot} \leq 74$ °C
$25 \leq T_c \leq 35$ °C

The parametric correlations developed in each case have been validated statistically by calculating a dimensionless parameter called the coefficient of determination (R^2) for each equation. It is defined as the fraction of the variability of the results obtained by the model [21]. An R^2 value close to 0 indicates that the model is a poor fit, while an R^2 value close to 1 demonstrates that the model is good [22]. However, a large value of R^2 does not necessarily implies that the regression model is a good one. R^2 often increases by adding irrelevant predictor variables to the regression equation [23, 24]. To compensate for this one, it is more valuable to take the adjusted R^2 (R_{adj}^2) into consideration, to check the correlation adequacy, which is defined as the variation of R^2 that reflects the number of terms in the model. Usually, the model that maximizes R_{adj}^2 is considered to be a good candidate for the best regression equation [25]. Cross-validation was used also to assess the fit with the $RMSE$ (also known as the standard error of the estimate). As its name suggests, the $RMSE$ is the root of the mean squared errors (i.e. take each error, square it, take the average of these squared errors, and then take the square root of this average) and it represents the magnitude of errors.

If it is negative then the procedure tends to under-predict values and when it is positive it indicates over-prediction. Ideally, then, the mean error would be 0, corresponding to accurate predictions [22]. Finally, an important parameter to assess the goodness of the fit is the error sum of squares (SSE). It is the difference of the actual response empirical values and the response values that is predicted from the fit. Just as with $RMSE$, a poor fit of data has a high SSE. A SSE value closer to 0 demonstrates that the model has a smaller random error component as a consequence the fit will be more valuable for prediction [26]. Table 12 summarizes the statistical results from the evaluation of the goodness of the fit. The values of $0.870 < R^2 < 0.993$ and $0.838 < R^2_{adj} < 0.990$ which are fairly high indicates that all the empirical correlations founded are good candidate to represent the behaviour of the distillate production and the PR in the solar MED plant. The values of $0.026 < RMSE < 0.169$ and $0.010 < SSE < 0.398$ which are small errors demonstrates that all the equations correspond to accurate predictions.

Table 12
The statistical results for the evaluation the goodness of fit

Statistical parameters	Eq. (7)	Eq. (8)	Eq. (9)	Eq. (10)	Eq. (11)	Eq. (12)
R^2	0.983	0.935	0.993	0.985	0.986	0.870
R^2_{adj}	0.978	0.897	0.990	0.971	0.984	0.838
$RMSE$	0.046	0.169	0.026	0.048	0.044	0.108
SSE	0.039	0.398	0.010	0.023	0.069	0.187

4. Conclusions and recommendations

The aim of this work is to perform an experimental characterization of a solar MED system under a wide range of operating conditions. Firstly, the assessment of the efficiency of a large-aperture FPC solar field has been carried out and thoroughly analyzed and plotted at several temperature levels for different climate conditions on the basis of meteorological data, the incidence angle calculated in Matlab and collected data from SCADA.

The experimental and theoretical efficiency results under test have revealed to be closed to each other. It was found that the mean experimental efficiency at $T_{out,SF}$ of 65 ºC was 43.1% greater than that of 95 °C. In addition, results of the analysis of the coupling of the MED plant with the solar field showed that the FPC solar field is able to produce more thermal power than required by the MED unit, especially at $T_{out,SF}$ of 65 °C when the thermal energy given by the solar field during the day was at its maximum, and these conditions allow to cover the operation of the MED plant during 6 hours, which includes the transient periods (clouds or start-up). Whereas, the operation of the solar field at higher temperatures ($T_{out,SF}$ of 95 ºC) permits the MED plant to operate during 4.4 hours.

In order to study the impact of several key parameters on the MED plant performance, three different cases have been concretely examined and valuable quantitative conclusions have been obtained. Table 13 indicates the optimum operation points that should be selected in function of the goal to be achieved: either the maximization of the distillate production or the minimization of the energetic consumption of the MED plant. The seasonal variation of the seawater temperature allows the operation of the MED plant at different T_c, being easier to operate at high T_c in summer months due to the high temperature of the seawater at this season. If the interest is to maximize the distillate production, in summer, it is more preferable to increase the m_f at the maximum value than increasing the m_{hot}, since it was proved that

the rise in the later has less impact in the distillate production than the rise in the former for the same T_{hot}. As the solar field can operate at high temperature in these months, and the rise in T_{hot} increases the distillate production, it is recommended to operate the solar field at the highest temperature ($T_{out,SF}$ at 95 ºC) to achieve a hot water temperature in the tanks such that it provides T_{hot} at 74 ºC to the MED plant. In winter months, it is recommended to operate at the minimum T_c and maximum $T_{out,SF}$ from the solar field, since it allows having the greatest distillate production. On the other hand, in cases in which the efficiency of the solar field and MED plant have to be maximized, the best operation strategy is to operate at intermediate T_{hot} at values of (66-68 ºC), keepingT_c, m_f and m_{hot} at 35 ºC, 8 m^3/h and 12 L/s, respectively. The results obtained can be useful as a benchmark to the community of solar desalination to perform characterization tests of solar MED units.

Table 13
Comparison of the optimum results of key parameters of the MED for the three study cases

Study cases	Hot water flow rate of (L/s)	Feed water flow rate (m^3/h)	Hot water inlet temperature (°C)	Condenser vapor temperature (°C)	Distillate production (m^3/h)	PR
Case study 1	12	8	74	35	2.95	9.42
	12	9	74	35	3.00	9.39
	12	8	68	35	2.73	11.10
Case study 2	7	8	60	35	1.77	9.71
	12	8	60	35	1.87	9.51
	12	8	70	35	2.62	8.83
Case study 3	12	8	66	35	2.49	9.80
	12	8	72	25	3.09	9.01
	12	8	74	25	3.22	8.89

Empirical correlations were successfully obtained and validated statistically in each case in order to predict the distillation production and the PR using a large range of validation. These equations can be used as an effective tool for the optimization of the solar MED systems and the selection of operating conditions in different seasons with the purpose of getting sustainable fresh water with an economic price.

Acknowledgments

This work has been funded by the Spanish Ministry of Economy and Competitiveness and ERDF funds under the National R+D+i Plan Project DPI2014-56364-C2-1-R and the 7th Framework Programme of the EU (SFERA 2 Grant Agreement n. 312643). Besides, the authors are thankful to “IRESEN” for providing financial support to realize this research under “Seawater desalination using solar energy project”, InnoTherm II Solar thermal applications and solar technologies support.

Nomenclature

Variables

A	The total aperture area of the collectors (m^2)
b_o	Incidence angle modifier coefficient (–)
β	Tilt angle (°)
C	The concentration ratio of areas (–)
E	Energy (kW)
G_T	Solar radiation (W/m^2)
h	Enthalpy (kJ/kg)
k_1	Heat loss coefficient (W/m^2K)
k_2	Temperature dependence of the heat loss coefficient (W/m^2K^2)
$K_{\tau\alpha}$	Incidence angle modifier (–)
M	Weight (kg)
$\dot{m}$	Flow rate of each loop (L/min)
$\dot{m}_d$	Distillate production mass flow rate (m^3/h)
m_f	Feed water mass flow rate (m^3/h)
m_{hot}	Hot water Flow rate (L/s)
η_0	Optical efficiency (%)
θ	Incident angle of the beam irradiance (°)
P	Power (kW_{th})
Q	Thermal energy (kW)
R^2	Coefficient of determination (–)
R^2_{adj}	Adjusted R^2 (–)
$RMSE$	Standard error of the estimate (–)
SS_E	Error sum of squares (–)
T	Temperature (°C)
T_{hot}	Hot water inlet temperature (°C)
U	Measurement uncertainties (–)

Acronyms and abbreviations

CPC	Compound parabolic concentrators
FPC	Flat Plat collector
HTTF	Horizontal tube thin film
LR	Load ratio
MED	Multiple effect distillation
PR	Performance ratio
PSA	Plataforma Solar de Almeria
TBT	Low top brine temperature
TES	Thermal energy storage

Subscripts

amb	Ambient
col	Average collector temperature
d	Distillate water
ex	Experimental
FPCs	Flat Plat collectors
hot	Hot water

in	Inlet
max	Maximum
mean	Mean value
out	Outlet
remaining	Remaining in the tank
supplied	Supplied by the SF
SF	Solar filed
th	Theoretical
U	Useful energy gain by the solar FPCs

References

[1] J. Blanco, D. Alarcón, E. Guillén, W. Gernjak, The AQUASOL system: solar collector field efficiency and solar-only mode performance, JSEE133 (2011) 011009-1.

[2] A.M. El-Nashar, Predicting part load performance of small MED evaporators - a simple simulation program and its experimental verification, Desalination 130 (2000) 217-234, ISSN: 0011-9164.

[3] P. Fernández-Izquierdo, L. García-Rodríguez, D.C. Alarcón-Padilla, P. Palenzuela, I. Martín-Mateos, Experimental analysis of a MED unit operated out of nominal conditions, Desalination 284 (2012) 233-237.

[4] P. Palenzuela, D. Alarcón, G. Zaragoza, Concentrating, Solar Power and Desalination Plants: Engineering and Economics of Coupling Multi-Effect Distillation and Solar Plants, Springer International Publishing (2015) VII, 172.

[5] D. Zhao, J.L. Xue, S. Li, Theoretical analyses of thermal and economical aspects of multi-effect distillation desalination dealing with high-salinity wastewater, Desalination 273(2/3) (2011) 292-298.

[6] J. L. Xue, Q. Cui, J. Ming, Y. Bai, L. Li, Analysis of Thermal Properties on Backward Feed Multieffect Distillation Dealing with High-Salinity Wastewater, Journal of Nanotechnology (1–3) (2015) 1-7.

[7] M. C. Georgiou, A. M. Bonanos, J.G. Georgiadis, Experimental evaluation of a multiple-effect distillation unit in low seawater flow conditions, Desalination and Water Treatment 55 (2015) 3267–3276.

[8] D. Zhao, T. Liu, J.L. Xue, S. Li, C. Li, W. Liu, H. Zhang, Y. Wang, A lab-scale MED dealing with salinity wastewater: the study of optimal operation schemes and parameters, Desalination and Water Treatment 57 (2015) 1–8.

[9] P. Palenzuela, A. S. Hassan, G. Zaragoza, D. C. Alarcon-Padilla, Steady state model for multi-effect distillation case study: Plataforma Solar de Almeria MED pilot plant, Desalination 337 (2014) 31-42.

[10] S. Fischer, W. Heidemann, H. Müller-Steinhagen, B. Perers, P. Bergquist, B. Hellström, Collector test method under quasi-dynamic conditions according to the European Standard EN 12975-2, Solar Energy 76 (1–3) (2004) 117-123.

[11] S.A. Kalogirou, Solar thermal collectors and applications, Progress in Energy and Combustion Science 30 (2004) 231–295.

[12] G. N. Tiwari, Solar Energy: Fundamentals, Design, Modeling and Applications, Pangbourne: Alpha Science, Print (2002).

[13] G.F. Nellis, S. A. Klein, Heat Transfer, Cambridge University Press, New York (2009).

[14] A. Saul, W. Wagner, International equations for the saturation properties of ordinary water substance, J. Phys. Chem. Ref. Data, 16 (4) (1987) 893–901.

[15] W. Wagner, A. Pruss, International equations for the saturation properties of ordinary water substance. Revised according to the international temperature scale of 1990, J. Phys. Chem. Ref. Data, 22 (3) (1993) 783–787.

[16] T. El-Dessouky, M. Ettouney, Multiple-effect evaporation desalination systems: thermal analysis, Desalination 125 (1999) 259-276.

[17] L. Yang, S. Shen, H.Hu, Thermodynamic performance of a low temperature multi-effect distillation experimental unit with horizontal-tube falling film evaporation, Desalination & Water Treatment 33: 1-3 (2011) 202-208.

[18] A.M. El-Nashar, AA. Qamhiyeh, Simulation of the steady-state operation of a multi-effect stack seawater distillation plant, Desalination 101 (1995) 231-43.

[19] J. Leblanc, J. Andrews, A. Akbarzadeh, Low-temperature solar-thermal multi-effect evaporation desalination systems, Int J Energy Res 34 (2010) 393-403.

[20] F. Kafi, V. Renaudin, D. Alonso, J. Hornut, M. Weber, Experimental study of a three-effect plate evaporator: Seawater tests in La Spezia, Desalination 182 (2005) 175–186.

[21] J. Paulo Davim, Design of Experiments in Production Engineering, Springer International Publishing, (2016) XI, 196.

[22] C. D. Lloyd, Spatial data analysis: an introduction for GIS users, Oxford University Press Inc., New York, (2010).
[23] S. J. Sheather, A Modern Approach to Regression with R, Springer, New York (2009).
[24] D. C. Montgomery, Design and analysis of experiments, 8th edition, John Wiley & Sons, Inc, New York (2012).
[25] D. C. Montgomery, G. C. Runger, Applied Statistics and Probability for Engineers, 6th Edition, Wiley (2014).
[26] MathWorks, Inc, Curve fitting toolbox 1: user's guide, MathWorks, 2006.